Modelling of heat transfer in computational fluid dynamics

OLLE BODIN

FOI
Defence Research Agency
Systems Technology
SE-164 90 Stockholm

Phone: +46 8 555 030 00
Fax: +46 8 555 031 00

www.foi.se

FOI-R--2079--SE Technical report
ISSN 1650-1942 August 2006

Systems Technology

Olle Bodin

Modelling of heat transfer in computational fluid dynamics

Issuing organisation FOI – Swedish Defence Research Agency Systems Technology SE-164 90 STOCKHOLM	**Report number, ISRN** FOI-R--2079--SE	**Report type** Technical report
	Research area code 7 Mobility and Space Technology, incl Materials	
	Month year August 2006	**Project no.** A 64032
	Sub area code 73 Air Vehicle Technologies	
	Sub area code 2	
Author/s (editor/s) Olle Bodin	**Project manager** Peter Eliasson	
	Approved by Monica Dahlen Head, Systems Technology	
	Sponsoring agency Swedish Department of Defence	
	Scientifically and technically responsible Stefan Wallin	
Report title Modelling of heat transfer in computational fluid dynamics		

Abstract

The scope of this thesis is to introduce advanced modelling of heat flux in turbulent flows into CFD. Explicit algebraic scalar flux modelling (EASFM) is considered and previous models are simplified in order to avoid near-wall damping functions and wall distance dependencies. The modification was verified by computations of fully developed channel flow with heat transfer. One of the original goals, to implement a EASFM into the research code of FOI (EDGE), could not be reached and the reason for this was related to numerical stability. The attempted implementation was analyzed, and a method to overcome the problems was proposed. The capability of the EDGE CFD code concerning numerical accuracy in the prediction of heat transfer using more standard heat flux models was assessed for fully developed turbulent channel flow. The code was found o be rather inaccurate for the combination of isothermal walls and low Mach number with regard to prediction of skin friction and wall heat flux. A comparison of several turbulence models as well as the two CFD solvers EDGE and Fluent was carried out using a plane impinging jet case with DNS data used for reference. Known model differences was confirmed and the low Mach number sensitivity of EDGE was also obvious here while Fluent better agreed with DNS data

Keywords

Computational fluid dynamics, impinging jet, wall heat flux, turbulent flow, algebraic scalar flux model

Further bibliographic information	**Language** English
ISSN ISSN-1650-1942	**Pages** 38 p.
	Price acc. to pricelist

Utgivare FOI – Totalförsvarets forskningsinstitut Systemteknik 164 90 STOCKHOLM	**Rapportnummer, ISRN** FOI-R--2079--SE	**Klassificering** Teknisk rapport
	Forskningsområde 7 Farkost- och rymdteknik, inkl material	
	Månad år Augusti 2006	**Projektnummer** A 64032
	Delområde 73 Flygfarkostteknik	
	Delområde 2	
Författare/redaktör Olle Bodin	**Projektledare** Peter Eliasson	
	Godkänd av Monica Dahlen Chef, Systemteknik	
	Uppdragsgivare/kundbeteckning Försvarsdepartementet	
	Tekniskt och/eller vetenskapligt ansvarig Stefan Wallin	

Rapportens titel
Modellering av värmetransport i strömningsmekaniska beräkningar

Sammanfattning

Detta examensarbete behandlar strömningsmekaniska beräkningar (CFD) med avancerad modellering av värmetransport i turbulent strömning. Så kallad *Explicit Algebraic Scalar Flux Modelling* (EASFM) behandlas med, i förhållande till tidigare försök, förenklade modeller. Modellerna saknar alla former av väggdistansberoende, något som funnits i tidigare försök med denna typ av modellering. Resultaten med den modifierade EASFM-modellen verifierades med beräkningar av fullt utvecklad turbulent kanalströmning med värmetransport. Ett av de ursprungliga målen med examensarbetet, att implementera en EASFM-modell i FOI's forskningskod (EDGE), kunde inte nås på grund av problem med numerisk stabilitet. Rapporten behandlar en analys av dessa problem och föreslår en lösning. Den numeriska noggrannheten hos EDGE vid analys av värmetransport, då mer standardmässiga modeller för värmetransport användes, utvärderades i ett fall av fullt utbildad turbulent kanalströmning. EDGE befanns vara relativt inexakt för kombinationen konstant väggtemperatur och låga Mach-tal vid analys av friktionen och värmeövergången vid väggarna i detta fall. Jämförelser mellan de två beräkningsprogrammen Fluent och EDGE samt mellan flera turbulensmodeller gjordes med hjälp av en plan jet där referensdata fanns i form av en DNS. Kända skillnader i modellernas beteende kunde observeras och även här var forskningskodens känslighet för låga Mach-tal tydlig medans Fluent bättre överensstämde med DNS-resultaten.

Nyckelord
Beräkningsaerodynamik, infallande jet, värmelast på vägg, turbulent strömning, algebraisk skalärflux-modellering

Övriga bibliografiska uppgifter	**Språk** Engelska
ISSN ISSN-1650-1942	**Antal sidor:** 38 s.
Distribution enligt missiv	**Pris: Enligt prislista**

Contents

1 Introduction

1.1 Background

The need for computational fluid dynamics, CFD, arises from the need to understand fluid flows and the effect they have on for example aircraft and also to better understand the physics of the flow itself. Most fluid flows in reality are turbulent making the understanding of turbulence very important in order to understand general fluid flows. One feature of turbulent flows that is very important in engineering applications is the turbulent transport of passive scalars e.g. heat. This report shall mainly deal with the modelling of this, specifically the use of a model developed by Wikström, Wallin and Johansson [3] which was further simplified by Högström Wallin and Johansson [15], [12]. In this study we will make further simplifications in order to avoid the near-wall damping functions in the modelling. The aim is to have a model that is robust and easily implemented into general CFD methods.

1.2 Characteristics of turbulence

Turbulence is not universally well understood and there are many definitions of its characteristics, this will be the authors attempt. Turbulence is characterized by chaotic, threedimensional fluctuations about a mean. In addition to this random behavior turbulence has a very large span in length-, and timescales. The largest of these scales are of the same size as the characteristic width of the flow making it dependent on flow boundary's and thus non universal.

Richardsson, an early contributor to high Re turbulence research, paraphrased J. Swift: "Big whorls have little whorls that feed on their velocity, and little whorls have lesser whorls and so on to viscosity- in a molecular sense" [1]. This later birthed the energy cascade models where turbulent energy is introduced at the largest scales and then transported by vortex stretching via the energy cascade to the smallest scales where the energy is then transferred to internal energy by dissipation.

Kolmogorov [2] introduced the idea that, for high Re, the energy producing scales, L, and the viscous dissipation scales, η, were widely separated. Building on this he then suggested that, in time-independent flow, the rate of production of turbulent energy at the large scales must be balanced by the rate of destruction at the small, viscous scales. These rates must also be equal to the flux of energy between these scales, ε, measured at any scale R in the inertial interval $\eta \ll R \ll L$. In the inertial interval, Kolmogorov suggested, ε is the only relevant parameter, and thus the only relevant length is R, η and L being irrelevant for the statistical characteristics of motion in the inertial range. This leads to three groups of scales: the viscous range, characterized by ε and the molecular viscosity ν, the inertial range and the energy containing range all having their own specifics requiring analysis.

In order to calculate the relevant properties of turbulent flows two approaches can be made: simulation or modelling. In contrast to modelling where equations for some mean quantity are solved simulation consists of solving equations for a time dependant velocity field describing one realization of the flow. Simulation consist of two general approaches: DNS (direct numerical simulation)and LES (large eddy simulation). In DNS the Navier-Stokes equations are solved and thus all time- and lengthscales must be resolved making this very computationally expensive and practically impossible for general, high Reynolds number, flows. In large eddy simulation a filtered velocity field representing the large scale turbulent motions is solved together with a model for the small scale motions making this less computationally expensive compared to DNS. Since modelling is needed for the small scales, LES can be considered as an intermediate step between simulation and modelling.

The chaotic, fluctuating nature of turbulence makes it plausible to treat with statistical methods and here the modelling approach to CFD comes in. If the variables in an incompressible flow is decomposed as

$$\hat{u}_i = U_i + u_i, \qquad \hat{p} = P + p, \qquad \hat{\theta} = \Theta + \theta \tag{1.1}$$

where U_i, P and Θ are the mean values of the velocity, pressure and passive scalar fields while u_i, p, θ are their respective turbulent fluctuations such that

$$\bar{\hat{u}}_i = U_i, \qquad \bar{\hat{p}} = P, \qquad \bar{\hat{\theta}} = \Theta \tag{1.2}$$

By definition the mean of the fluctuating part is equal to zero and this process is called Reynolds decomposition. By ensamble averaging the Navier-Stokes equation

$$\frac{\partial \hat{u}_i}{\partial t} + \hat{u}_j \frac{\partial \hat{u}_i}{\partial x_j} = -\frac{1}{\rho}\frac{\partial \hat{p}}{\partial x_i} + \frac{\partial}{\partial x_j}\left(\nu \frac{\partial \hat{u}_i}{\partial x_j}\right) \tag{1.3}$$

and the transport equation for a passive scalar

$$\frac{\partial \hat{\theta}}{\partial t} + \hat{u}_j \frac{\partial \hat{\theta}}{\partial x_j} = \frac{\partial}{\partial x_j}\left(\alpha \frac{\partial \hat{\theta}}{\partial x_j}\right) \tag{1.4}$$

by using Reynolds decomposition the Reynolds averaged transport equation for the velocity and scalar field are obtained.

$$\frac{\partial U_i}{\partial t} + U_j \frac{\partial U_i}{\partial x_j} = -\frac{1}{\rho}\frac{\partial P}{\partial x_i} + \frac{\partial}{\partial x_j}\left[\nu\left(\frac{\partial U_i}{\partial x_j} + \frac{\partial U_j}{\partial x_i}\right) - \overline{u_i u_j}\right] \tag{1.5}$$

$$\frac{\partial \Theta}{\partial t} + U_j \frac{\partial \Theta}{\partial x_j} = \frac{\partial}{\partial x_j}\left(\alpha \frac{\partial \Theta}{\partial x_j} - \overline{u_j \theta}\right) \tag{1.6}$$

The last term in the respective expressions are from top to bottom the Reynolds stress tensor and the Reynolds scalar flux vector which result from the nonlinearity in the advection term. These correlations need to be modeled in order to solve (1.5) and (1.6).

There are many models for these two correlations but historically it all stared with the turbulent viscosity hypothesis and the gradient diffusion hypothesis for the stresses and the flux vector, respectively.

$$-\overline{u_i u_j} = \nu_T\left(\frac{\partial U_i}{\partial x_j} + \frac{\partial U_j}{\partial x_i}\right) - \frac{2}{3}K\delta_{ij} \tag{1.7}$$

$$-\overline{u_i \theta} = \frac{\nu_T}{Pr_T}\frac{\partial \Theta}{\partial x_i} \tag{1.8}$$

2 The scalar flux models

2.1 Eddy-diffusivity model

In order to have a straightforward, relatively simple model to aid in implementation and as a reference the eddy-diffusivity model (EDM) was used to model the passive scalar flux.

$$-\overline{u_i\theta} = \alpha_T \frac{\partial \Theta}{\partial x_i}, \qquad \alpha_T = \frac{\nu_T}{Pr_T} \tag{2.1}$$

Above α_T, ν_T and Pr_T are the eddy diffusivity, eddy viscosity and the turbulent Prantl number respectively. The eddy viscosity can be modeled in several ways, in this case with the help of a $k-\omega$ model so that it is dependent on the balance between turbulent kinetic energy and the dissipation of turbulent kinetic energy.

$$\nu_T = \frac{k}{\omega} \tag{2.2}$$

2.2 Explicit algebraic scalar flux model

A more accurate way to model the passive scalar flux is to use a model that does not assume the scalar flux to be aligned with the mean scalar gradient.

$$\overline{u_i\theta} = -(1-c_{\theta 4})A_{ij}^{-1}\overline{u_j u_k}\frac{k}{\varepsilon}\frac{\partial \Theta}{\partial x_k} \tag{2.3}$$

The equation (2.3) is one such model, a so called explicit algebraic scalar flux model (EASFM) by Wikström et al. [3]. It utilizes an algebraic relation for the passive scalar flux consisting of mean flow quantities by an equilibrium condition in the transport equations for the normalized passive scalar flux. If the velocity and scalar gradients are large, this is a reasonable assumption This approach to scalar flux modelling is analogous to explicit algebraic Reynolds stress modelling, briefly touched in the next chapter, for the Reynolds stress anisotropies. In general, the assumption that the advection and diffusion of the scalar flux is negligible gives an nonlinear, implicit set of algebraic equations. The way around this problem used by Wikström et al. [3] was to use a nonlinear term, the $c_{\theta 5}$ term, in the model of the pressure scalar-gradient correlation and molecular destruction. With the particular choice of $c_{\theta 5} = 1/2$ the nonlinearity will be cancelled out.

$$\begin{aligned}\Pi_{\theta i} - \varepsilon_{\theta i} = &-\left(c_{\theta 1} + c_{\theta 5}\frac{k}{\varepsilon k_\theta}\overline{u_k\theta}\frac{\partial \Theta}{x_k}\right)\frac{\varepsilon}{k}\overline{u_i\theta} + c_{\theta 2}\overline{u_j\theta}\frac{\partial U_i}{\partial x_j} \\ &+ c_{\theta 3}\overline{u_j\theta}\frac{\partial U_j}{\partial x_i} + c_{\theta 4}\overline{u_i u_j}\frac{\partial \Theta}{\partial x_j},\end{aligned} \tag{2.4}$$

In equation (2.4) k_θ is the half scalar variance, defined as

$$k_\theta \equiv \frac{\overline{\theta}^2}{2}. \tag{2.5}$$

Now, with a clever choice of model constants and some algebra the model (2.3) was obtained. Most of the terms in equation (2.3) are recognizable such as $\overline{u_j u_k}$ (Reynolds stress), k (turbulent kinetic energy), ε (dissipation of turbulent kinetic energy) and $\partial\Theta/\partial x_k$ (gradient of the mean passive scalar) but A and $c_{\theta 4}$ are not. The latter is a constant used for calibration of the model while A is a second rate tensor $\mathbf{A} \equiv A_{ij}$:

$$A_{ij} = N_\theta \delta_{ij} + c_S S_{ij} + c_\Omega \Omega_{ij}, \tag{2.6}$$

where

$$N_\theta = G + \frac{1}{r}\frac{\mathcal{P}_\theta}{\varepsilon_\theta}\left(\frac{1}{2} - c_{\theta 5}\right) \tag{2.7}$$

$$G = \frac{1}{2}\left(2c_{\theta 1} - 1 - \frac{1}{r} + \frac{\mathcal{P}_K}{\varepsilon}\right) \tag{2.8}$$

and

$$S_{ij} = \frac{1}{2}\frac{k}{\varepsilon}\left(\frac{\partial U_i}{\partial x_j} + \frac{\partial U_j}{\partial x_i}\right), \qquad \Omega_{ij} = \frac{1}{2}\frac{k}{\varepsilon}\left(\frac{\partial U_i}{\partial x_j} - \frac{\partial U_j}{\partial x_i}\right) \tag{2.9}$$

In (2.7) the choice $c_{\theta 5} = \frac{1}{2}$ makes N_θ equal to G leading to a less complex model, in this report this choice of $c_{\theta 5}$ will be used. In order to obtain the inverse of $\mathbf{A}$ the so called *Cayley-Hamilton theorem* is used. This theorem says that any square matrix satisfies its own characteristic equation. In the case of $\mathbf{A}$ it reads:

$$\mathbf{A}^3 - \mathrm{tr}\{\mathbf{A}\}\mathbf{A}^2 + \frac{1}{2}\left(\mathrm{tr}\{\mathbf{A}\}^2 - \mathrm{tr}\{\mathbf{A}^2\}\right)\mathbf{A} - \det(\mathbf{A})\mathbf{I} = \mathbf{0}, \tag{2.10}$$

Here $\mathbf{I}$ is the identity matrix, $\det(\mathbf{A})$ and $\mathrm{tr}\{\mathbf{A}\}$ are the determinant and trace of $\mathbf{A}$ respectively. To obtain $\mathbf{A}^{-1}$ both sides of (2.10) are multiplied by $\mathbf{A}^{-1}$

$$\mathbf{A}^{-1} = \frac{\frac{1}{2}\left(\mathrm{tr}\{\mathbf{A}\}^2 - \mathrm{tr}\{\mathbf{A}^2\}\right)\mathbf{I} - \mathrm{tr}\{\mathbf{A}\}\mathbf{A} + \mathbf{A}^2}{\det(\mathbf{A})}. \tag{2.11}$$

Now (2.6) is inserted into (2.11) yielding:

$$\mathbf{A}^{-1} = \frac{\left(G^2 - \frac{1}{2}Q_1\right)\mathbf{I} - G\left(c_S\mathbf{S} + c_\Omega\mathbf{\Omega}\right) + \left(c_S\mathbf{S} + c_\Omega\mathbf{\Omega}\right)^2}{G^3 - \frac{1}{2}GQ_1 + \frac{1}{2}Q_2}, \tag{2.12}$$

where the invariants of the mean flow gradients are,

$$II_S \equiv \mathrm{tr}\{\mathbf{S}^2\}, \quad II_\Omega \equiv \mathrm{tr}\{\mathbf{\Omega}^2\}, \quad III_S \equiv \mathrm{tr}\{\mathbf{S}^3\}, \quad IV \equiv \mathrm{tr}\{\mathbf{S}\mathbf{\Omega}^2\}, \tag{2.13}$$

$$Q_1 \equiv c_S^2 II_S + c_\Omega^2 II_\Omega, \qquad Q_2 \equiv \frac{2}{3}c_S^3 III_S + 2c_S c_\Omega^2 IV. \tag{2.14}$$

The term k/ε, describing a turbulent timescale, is replaced with a timescale proposed by Durbin [5] which gives a more physically correct description near and on the wall.

$$\tau = \max\left(\frac{k}{\varepsilon}, C_\tau\sqrt{\frac{\nu}{\varepsilon}}\right), \qquad C_\tau = 6.0 \tag{2.15}$$

The model constants are defined as follows:

$$c_S = 1 - c_{\theta 2} - c_{\theta 3} \tag{2.16}$$

$$c_\Omega = 1 - c_{\theta 2} + c_{\theta 3} \tag{2.17}$$

$$c_{\theta 1} = c'_{\theta 1}\frac{r+1}{r} \tag{2.18}$$

where r is the scalar to dynamic time ratio defined as

$$r = \frac{k_\theta/\varepsilon_\theta}{k/\varepsilon} \tag{2.19}$$

where ε_θ is the destruction of k_θ, the half scalar variance. Depending on the value of these constants the model will of course behave differently. In this work a set of constants used by Högström et al. [15] were used such as

$$\begin{aligned} c_{\theta 1} &= 4.51 \quad c_{\theta 2} = -0.47 \quad c_{\theta 3} = 0.020 \\ c_{\theta 4} &= 0.08 \quad\quad c_{\theta 5} = 0.5 \end{aligned}$$

In order for the model to better predict the gradient in the center of the channel an approximation of the diffusion term is added to (2.7). The constant $C_{D\theta}$ is set to 6.7 to get the best possible agreement with DNS data. This value is slightly different to the one used by Högström et al. [15], $C_{D\theta} = 8.0$, because of the approach used in this report.

$$N_\theta = \frac{1}{2}\left(2c_{\theta 1} - 1 - \frac{1}{r} + \frac{\mathcal{P}_K}{\varepsilon}\right) + C_{D\theta}\max\left(1 - \frac{\mathcal{P}_K}{\varepsilon}, 0\right) \tag{2.20}$$

Now all the parts of (2.3) are defined in terms of the flow variables. The model by Högström et al. [12] was used together with the Wallin & Johansson [4] explicit algebraic Reynolds stress model that is able to make reasonably correct predictions of all Reynolds stress components and also their near-wall behavior. In this study we will use the EARSM with simplified near-wall treatment, without any near-wall damping functions or wall distance dependency, in order to have a version that is more attractive in implementation and use in industrial CFD solvers. The drawback is, thus, that the near-wall behavior for the Reynolds stress tensor and heat flux vector cannot be expected to be very accurate.

3 The turbulence models

In this report two turbulence models have been used: the Wilcox $k-\omega$ model and the Wallin and Johansson EARSM model together with the Hellsten $k-\omega$ model. This chapter will give a brief description of them and their use.

3.1 Wilcox $k-\omega$

The Wilcox or standard $k-\omega$ model is, together with the $k-\varepsilon$ model, the most widely used two equation models. Like the name implies it consists of equations which are solved for the turbulent variables k and ω

$$\frac{Dk}{Dt} = \frac{\partial}{\partial x_j}\left(\left(\nu + \frac{\nu_T}{\sigma_k}\right)\frac{\partial k}{\partial x_j}\right) + \mathcal{P} - \varepsilon \tag{3.1}$$

$$\frac{D\omega}{Dt} = \frac{\partial}{\partial x_j}\left(\left(\nu + \frac{\nu_T}{\sigma_\omega}\right)\frac{\partial \omega}{\partial x_j}\right) + \gamma\frac{\mathcal{P}\omega}{k} - \beta\omega^2 \tag{3.2}$$

γ, β, σ_k and σ_ω are model constants defined further down. Now with the dissipation rate defined as

$$\varepsilon \equiv \beta^*\omega k \tag{3.3}$$

the turbulent viscosity

$$\nu_T = \frac{k}{\omega} \tag{3.4}$$

and the production of turbulent kinetic energy

$$\mathcal{P} \equiv -\overline{u_i u_j}\frac{\partial U_i}{\partial x_j} \tag{3.5}$$

only the eddy viscosity hypothesis is now needed to make the $k-\omega$ model complete. It is defined as

$$\overline{u_i u_j} = \frac{2}{3}k\delta_{ij} - 2\nu_T S^*_{ij} \tag{3.6}$$

where

$$S^*_{ij} = \frac{1}{2}\left(\frac{\partial U_i}{\partial x_j} + \frac{\partial U_j}{\partial x_i}\right) \tag{3.7}$$

Finally the model constants are

Model constant	Value
σ_k	2.0
σ_ω	2.0
γ	5/9
β	3/40

3.2 Wallin & Johansson EARSM with Hellsten $k-\omega$

The Hellsten $k-\omega$ model [14] was created specifically to be used together with the W & J EARSM model as a scale determining two equation model in high lift aerodynamic CFD applications. As it differs on many points from Wilcox $k-\omega$ it is presented in detail.

$$\frac{Dk}{Dt} = \frac{\partial}{\partial x_j}\left(\left(\nu + \frac{\nu_T}{\sigma_k}\right)\frac{\partial k}{\partial x_j}\right) + \mathcal{P} - \varepsilon \tag{3.8}$$

$$\frac{D\omega}{Dt} = \frac{\partial}{\partial x_j}\left(\left(\nu + \frac{\nu_T}{\sigma_\omega}\right)\frac{\partial \omega}{\partial x_j}\right) + \gamma\frac{\mathcal{P}\omega}{k} - \beta\omega^2 + \\ + \frac{\sigma_d}{\omega}\max\left(\frac{\partial k}{\partial x_j}\frac{\partial \omega}{\partial x_j}; 0\right) \tag{3.9}$$

Similarly to the $k-\omega$ models by Menter [13] this model uses a mixing function to better deal with the differences in fluid behavior at different distances to the walls. The mixing function varies the model constants in space as a function of the wall distance. The model coefficients will vary in space according to

$$\begin{pmatrix} \gamma \\ \beta \\ \sigma_k \\ \sigma_\omega \\ \sigma_d \end{pmatrix} = f_{mix}\begin{pmatrix} \gamma_1 \\ \beta_1 \\ \sigma_{k1} \\ \sigma_{\omega 1} \\ \sigma_{d1} \end{pmatrix} + (1 - f_{mix})\begin{pmatrix} \gamma_2 \\ \beta_2 \\ \sigma_{k2} \\ \sigma_{\omega 2} \\ \sigma_{d2} \end{pmatrix} \tag{3.10}$$

and have the following numeric values

Model constant	set 1	set 2
γ	0.518	0.44
β	0.0747	0.0828
σ_k	0.91	0.91
σ_ω	1.89	1.0
σ_d	1.0	0.4

while γ_1, β_1 and $\sigma_{\omega 1}$ are related through the log-law relation

$$\gamma_1 = \frac{\beta_1}{\beta^*} - \frac{\kappa^2\sigma_{\omega 1}}{\sqrt{\beta^*}} \tag{3.11}$$

with $\beta^* = 0.09$ and $\kappa = 0.42$. The mixing function is defined as

$$f_{mix} = \tanh(C_{mix}\Gamma^4), \qquad \Gamma = \min(\max(\Gamma_1; \Gamma_2); \Gamma_3) \tag{3.12}$$

with the arguments

$$\Gamma_1 = \frac{\sqrt{k}}{\beta^*\omega d} \tag{3.13}$$

$$\Gamma_2 = \frac{500\nu}{\omega d^2} \tag{3.14}$$

$$\Gamma_3 = \frac{20k}{\max(d^2(\nabla k \cdot \nabla\omega)/\omega; 200k_\infty)} \tag{3.15}$$

where d is the distance to the wall and $C_{mix} = 1.5$. The Reynolds stresses are modeled through the Reynolds stress anisotropy tensor defined as

$$a_{ij} = \frac{\overline{u_i u_j}}{k} - \frac{2}{3}\delta_{ij} \tag{3.16}$$

but to make implementation of the model into CFD solvers more practical the model is instead expressed using eddy viscosity formulation with an extra anisotropy tensor.

$$\overline{u_i u_j} = \frac{2}{3}k\delta_{ij} - 2\nu_t S^*_{ij} + k a^{(ex)}_{ij}. \tag{3.17}$$

The effective eddy viscosity reads

$$\nu_T = C_\mu k\tau, \qquad C_\mu = -\frac{1}{2}(\beta_1 + II_\Omega\beta_6) \tag{3.18}$$

and the extra anisotropy

$$\begin{aligned} a^{(ex)}_{ij} &= a_{ij} - (\beta_1 + II_\Omega\beta_6)S_{ij} \\ &+ \beta_3\left(\Omega_{ik}\Omega_{kj} - \frac{1}{3}II_\Omega\delta_{ij}\right) + \beta_4\left(S_{ik}\Omega_{kj} - \Omega_{ik}S_{kj}\right) \\ &+ \beta_6\left(S_{ik}\Omega_{kl}\Omega_{lj} + \Omega_{ik}\Omega_{kl}S_{lj} - II_\Omega S_{ij} - \frac{2}{3}IV\delta_{ij}\right) \\ &+ \beta_9\left(\Omega_{ik}S_{kl}\Omega_{lm}\Omega_{mj} - \Omega_{ik}\Omega_{kl}S_{lm}\Omega_{mj}\right) \end{aligned} \tag{3.19}$$

In equation (3.19) S and Ω are the nondimensional strainrate and vorticity tensors defined in equation (2.9) and used with the Durbin time scale, equation (2.15). The mean flow invariants, II_Ω and IV are defined in equations (2.13). The coefficients β_x are functions of these invariants as

$$\begin{aligned} \beta_1 &= -\frac{N\left(2N^2 - 7II_\Omega\right)}{Q}, \quad \beta_3 = -\frac{12N^{-1}IV}{Q}, \\ \beta_4 &= -\frac{2\left(N^2 - 2II_\Omega\right)}{Q}, \quad \beta_6 = -\frac{6N}{Q}, \quad \beta_9 = \frac{6}{Q}, \end{aligned} \tag{3.20}$$

with the non-singular denominator

$$Q = \frac{5}{6}\left(N^2 - 2II_\Omega\right)\left(2N^2 - II_\Omega\right). \tag{3.21}$$

For two-dimensional flows N is solved from a cubic equation.

$$N = \frac{A_3^{'}}{3} + \begin{cases} \left(P_1 + \sqrt{P_2}\right)^{1/3} + \text{sign}\left(P_1 - \sqrt{P_2}\right)|P_1 - \sqrt{P_2}|^{1/3}, & P_2 \geq 0, \\ 2\left(P_1^2 - P_2\right)^{1/6}\cos\left[\frac{1}{3}\arccos\left(\frac{P_1}{\sqrt{P_1^2 - P_2}}\right)\right], & P_2 < 0, \end{cases} \tag{3.22}$$

In three dimensions the equation for N is of the sixth order and without an explicit solution. The treatment of three dimensional cases will not be assessed here as it is a much more complicated case, for more information see [3]. P_1 and P_2 are defined as follows

$$\begin{aligned} P_1 &= \left(\frac{A_3^{'\,2}}{27} + \frac{9}{20}II_S - \frac{2}{3}II_\Omega\right)A_3^{'}, \\ P_2 &= P_1^2 - \left(\frac{A_3^{'\,2}}{9} + \frac{9}{10}II_S + \frac{2}{3}II_\Omega\right)^3, \end{aligned} \tag{3.23}$$

and

$$A_3^{'} = \frac{9}{5} + \frac{9}{5}C_{Diff}\max\left(1 + \beta_1^{(eq)}II_S; 0\right), \tag{3.24}$$

where the second term models the otherwise ignored diffusion in the anisotropy. The parameter $\beta_1^{(eq)}$ is defined as

$$\beta_1^{(eq)} = -\frac{6}{5}\frac{N^{(eq)}}{(N^{(eq)})^2 - 2II_\Omega} \tag{3.25}$$

and with

$$N^{(eq)} = \frac{81}{20}, \qquad C_{Diff} = 2.2 \tag{3.26}$$

4 General 1D-solver and channel computations

To aid in testing of the models and to provide reference results a general 1D-solver for partial differential equations was used. The solver uses a MAPLE [6] worksheet to input equations, constants, boundary and initial conditions. Because of this the input of complicated tensor expressions can be made in a symbolic way which, in turn, greatly shortens debugging time and allows the user to focus more on the physics of the problem. Special Maple routines then produce Fortran code which can be compiled in order to solve the problem.

4.1 Implementation of the equations

The expression (1.6) shows the general (tensor) form of the Reynolds averaged transport equation for a passive scalar which can be simplified for the fully developed channel flow case that the program was made for. All derivatives with respect to x as well as the mean velocity in the y-direction are equal to zero and this leaves us with

$$\frac{\partial \Theta}{\partial t} = \frac{\partial}{\partial y}\left(\alpha \frac{\partial \Theta}{\partial y} - \overline{v\theta}\right) \tag{4.1}$$

where the term $-\overline{v\theta}$, the passive scalar flux, needs to be modelled. Actually, as the flow is also stationary the derivative with respect to time is also zero, but it will be left as it is for reasons explained later.

4.1.1 Eddy-diffusivity model

In this case one has only to combine (4.1) with (2.1) to get an expression ready for the 1D-solver.

$$\frac{\partial \Theta}{\partial t} = \frac{\partial}{\partial y}\left((\alpha + \alpha_T)\frac{\partial \Theta}{\partial y}\right) \tag{4.2}$$

or, in a more general form

$$\frac{\partial \Theta}{\partial t} = \frac{\partial}{\partial y}\left((\frac{\nu}{Pr} + \frac{\nu_T}{Pr_T})\frac{\partial \Theta}{\partial y}\right) \tag{4.3}$$

where ν and Pr are the viscosity and the Prantl number respectively.

4.1.2 Explicit algebraic scalar flux model

As i in (2.3) is equal to 2 in this example the expression (2.3) is simplified to

$$\overline{v\theta} = -(1 - c_{\theta 4})A_{2_j}^{-1}\overline{u_j u_k}\frac{k}{\varepsilon}\frac{\partial \Theta}{\partial x_k} \tag{4.4}$$

and, as all derivatives with respect to x are equal to zero (4.4) is expanded to

$$\overline{v\theta} = -(1 - c_{\theta 4})\frac{k}{\varepsilon}\frac{\partial \Theta}{\partial y}\left(A_{21}^{-1}\overline{uv} + A_{22}^{-1}\overline{v}^2\right) \tag{4.5}$$

with

$$A_{21}^{-1} = \frac{\mathrm{tr}\{\mathbf{A}\}\mathbf{A}_{21} + \mathbf{A}_{21}^2}{\det(\mathbf{A})} \tag{4.6}$$

$$A_{22}^{-1} = \frac{\frac{1}{2}(\mathrm{tr}\{\mathbf{A}\}^2 - \mathrm{tr}\{\mathbf{A}^2\}) - \mathrm{tr}\{\mathbf{A}\}\mathbf{A}_{22} + \mathbf{A}_{22}^2}{\det(\mathbf{A})} \tag{4.7}$$

where

$$\mathbf{A} = \begin{pmatrix} N_\theta & \frac{k}{2\varepsilon}\frac{\partial U}{\partial y}(c_S + c_\Omega) & 0 \\ \frac{k}{2\varepsilon}\frac{\partial U}{\partial y}(c_S - c_\Omega) & N_\theta & 0 \\ 0 & 0 & N_\theta \end{pmatrix} \tag{4.8}$$

so

$$\mathrm{tr}\{\mathbf{A}\} = 3N_\theta \tag{4.9}$$

$$\det(\mathbf{A}) = N_\theta(N_\theta^2 - \left(\frac{k}{2\varepsilon}\frac{\partial U}{\partial y}\right)^2 (c_S^2 - c_\Omega^2)) \tag{4.10}$$

$$\mathrm{tr}\{\mathbf{A}^2\} = 3N_\theta^2 + \left(\frac{k}{\varepsilon}\frac{\partial U}{\partial y}\right)^2 (c_S^2 - c_\Omega^2)) \tag{4.11}$$

Now everything is identified and (4.1) changes to

$$\frac{\partial \Theta}{\partial t} = \frac{\partial}{\partial y}\left((\alpha + \alpha_T^{eff})\frac{\partial \Theta}{\partial y}\right) \tag{4.12}$$

where the effective diffusivity, in this specific case of fully developed channel flow, becomes.

$$\alpha_T^{eff} = (1 - c_{\theta 4})\tau\left(A_{21}^{-1}\overline{uv} + A_{22}^{-1}\overline{v}^2\right) \tag{4.13}$$

4.2 Implementations of scalar flux models in the general 1D-solver

The 1D-solver inputs are algebraic equations in a MAPLE worksheet, the equations must be on the form

$$\frac{\partial \mathbf{q}}{\partial t} = \mathbf{f}\left(\mathbf{q}, \frac{\partial \mathbf{q}}{\partial y}, \frac{\partial^2 \mathbf{q}}{\partial y^2}, \ldots\right) \tag{4.14}$$

where $\mathbf{q}$ is a vector of unknowns. Now the reason for keeping the derivative with respect to time in (4.1) is obvious, it is the way in which the program reads the input.

4.3 Grid

The grid consists of two mirrored halves with 100 grid points and a stretch factor of 1.04 and thus have a total of 201 points. The thickness of the fist cell in wall units is $\Delta y^+ = 0.02$.

4.4 Calculations

As the main reasons for the 1D computations were to obtain results for comparison and to familiarize with the model and the implementation of it this section will not go into any details concerning the behavior of the models or the solver. A more detailed analysis of the model and its behavior with the 1D-solver can be found in the report by Högström [12].

4.4.1 Eddy-diffusivity model

The EDM model predicts the mean scalar profile for DNS data rather well, see figure 4.1. The $\overline{u\theta}$ component of the scalar flux, however, is not well predicted as this model assumes that it is zero. This, of course, is because the EDM model predicts the entire flux parallel to the mean scalar gradient which in this case is perpendicular to the walls. It is clear that in this case such a simplification of the scalar flux excludes important characteristics of the flow. The $\overline{u\theta}$ is in fact larger by some degree and can be expected to play a significant role in the scalar transport of turbulent boundary layers in cases where the mean flow variation in the streamwise direction is significant. The T^+ plot shows that the DNS and EDM agree rather well up to $y^+ \cong 10$ when they start to deviate. This however, is not because of the absence of $\overline{u\theta}$ but of the the erroneous prediction of $\overline{v\theta}$. As a conclusion the EDM model in this case can be said to predict mean scalar profiles well, as well as the $\overline{v\theta}$ component of the scalar flux. The simplicity of the model however, sacrifices physical correctness. The most obvious example is of course the complete absence of the $\overline{u\theta}$ component of the scalar flux something that will cause problems if the mean flow variation in the streamwise direction is significant.

4.4.2 Explicit algebraic scalar flux model

In figure 4.2, results from the EASFM model show clearly that this model is a lot more physically correct than the EDM. Here, just as with the EDM, the mean scalar profile is well predicted but unlike the EDM the $\overline{u\theta}$ component is not predicted equal to zero. The model fails to accurately predict $\overline{u\theta}$ close to the wall. This is due to the simplified near-wall treatment used in this study in both the $k-\omega$ model as well as in the EASFM and is, thus, related to the underestimation of k by the EARSM as can be seen in the bottom of figure 4.3. This can be corrected by using damping functions as in the report by Högström [12]. Such functions are typically calibrated for channel flow which, if one then wants to use it somewhere else, makes it necessary to make assumptions about the calculated flow. To use the fact that turbulence is universal at a certain scale, the inner layer, to motivate the use of the functions in general cases is perhaps not the most far flung of ideas but non the less widely used. In this report the EARSM and the $k-w$ model, as well as the EASFM, are free of damping functions making them more simple. Unfortunately in this case they are not accurate enough to allow the correct prediction of $\overline{u\theta}$ but since the mean scalar profile is not directly influenced by $\overline{u\theta}$, only by $\overline{v\theta}$, this deficiency might be considered acceptable. Altough the $\overline{u\theta}$ component does not affect the mean profile the EASFM model is still a better, more physically correct, model than the EDM evident in the T^+ plot in which the EARSM data better agrees with the DNS compared to the EDM. To conclude the EASFM model is better than the EDM in every way except simplicity. An EASFM requires a turbulence model that predicts the individual Reynolds stresses as correctly as possible in order to fully utilize the potential of the model and this is in this case obtained by the EARSM approach.

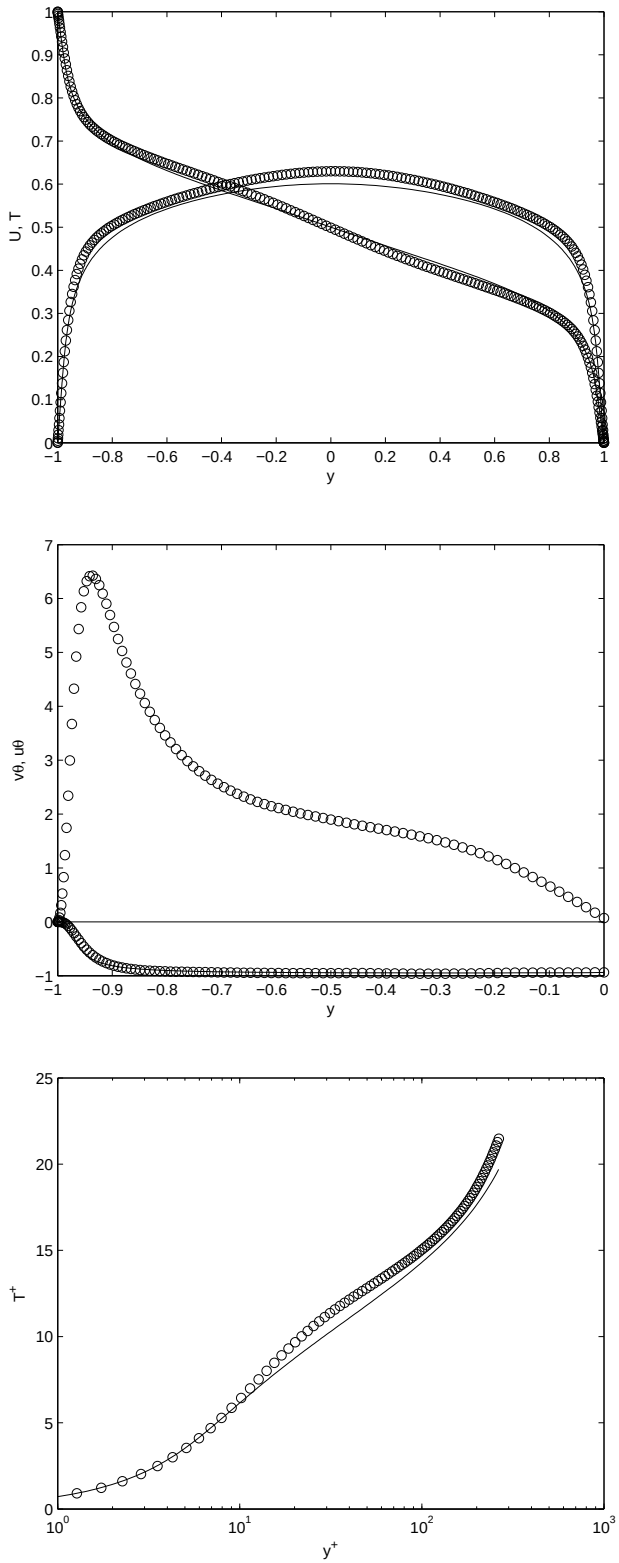

Figure 4.1: Eddy-diffusivity model , Top: $\circ$, Θ and U from DNS; — , Θ and U from EDM; Middle: $\circ$, $v\theta$ and $u\theta$ from DNS; — , $v\theta$ and $u\theta$ from EDM; Bottom: $\circ$, T^+ from DNS; — ,T^+ from EDM

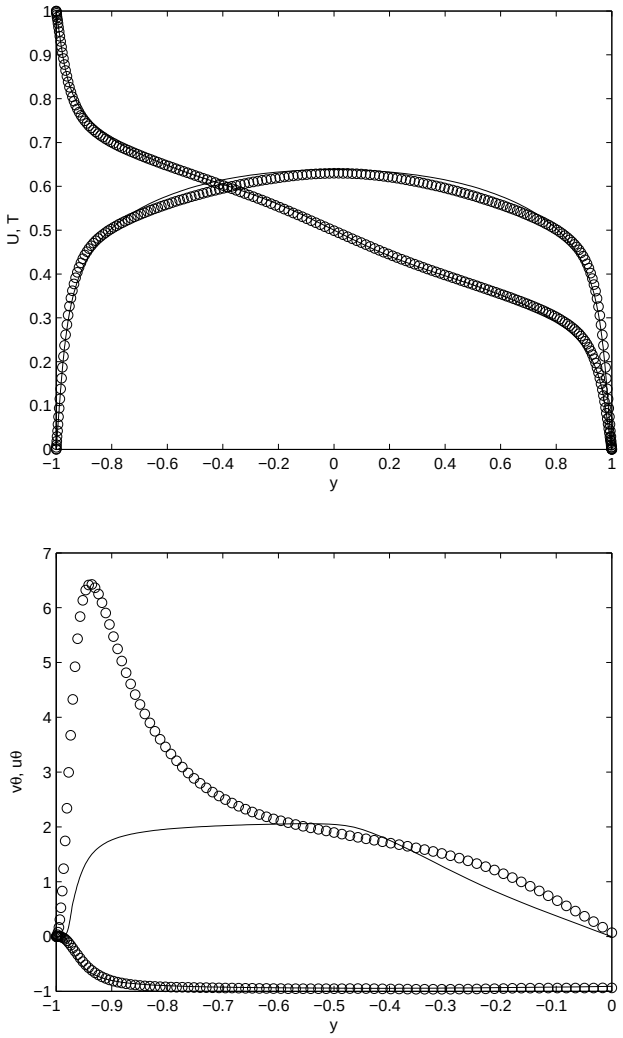

Figure 4.2: HJJW EASFM with EARSM and DM, $CD_\Theta = 6.7$, Top: $\circ$, Θ and U from DNS; — , Θ and U from HJJWd + DM; Bottom: $\circ$, $v\theta$ and $u\theta$ from DNS; — , $v\theta$ and $u\theta$ from HJJWd + DM;

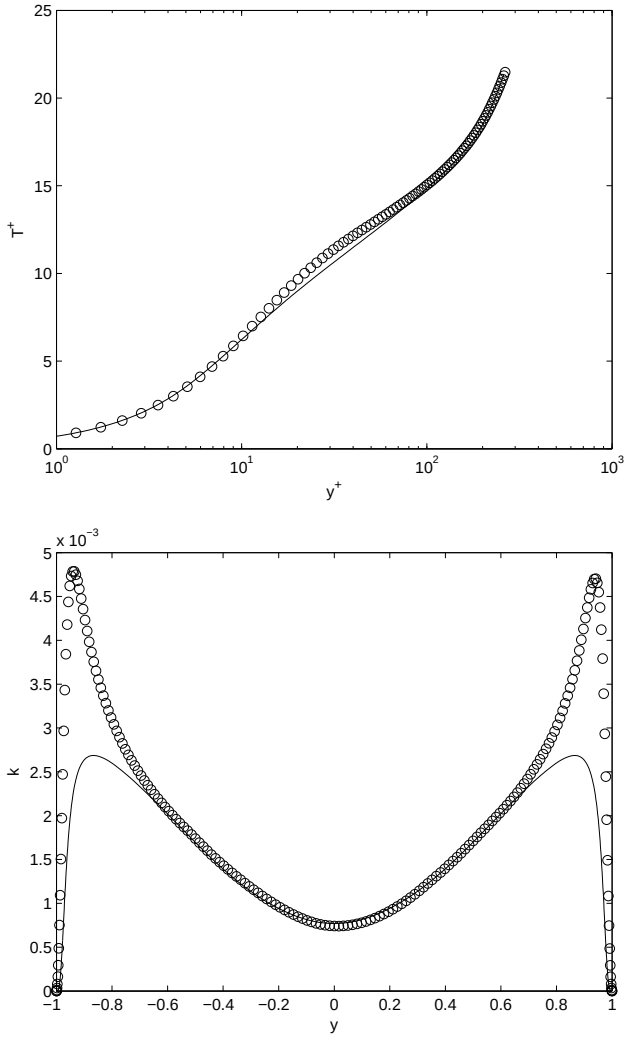

Figure 4.3: HJJW EASFM with EARSM and DM, $CD_\Theta = 6.7$, Top: $\circ$, T^+ from DNS; — ,T^+ from HJJWd + DM; Bottom: $\circ$, k from DNS; — ,k from HJJWd + DM

5 EDGE calculations

5.1 Introduction

EDGE is a parallelized CFD flow solver system developed by FOI [8], [9]. It is capable of 2D/3D viscous/inviscid, compressible flow problems on unstructured grids with arbitrary elements. The flow solver employs an edge-based formulation which uses a node-centered finite-volume technique to solve the governing equations. The control volumes are non-overlapping and are formed by a dual grid, which is computed from the control surfaces for each edge of the primary input mesh. In the flow solver, the governing equations are integrated explicitly towards steady state by Rung - Kutta time integration. Convergence is accelerated using agglomeration multigrid and implicit residual smoothing. The implementation of the EASFM model into EDGE adds a new functionality to the code. For the edge-calculations gridgeneration was handled by an FFA-developed gridgenerator, FFANET [7]. The program produces structured 2D/3D multiblock grids by transfinite interpolation and elliptic smoothing.

5.2 Fully developed turbulent channel flow

Because of availability of both DNS and 1D-solver data fully developed channel flow was chosen as a first testcase for the EASFM in EDGE

5.2.1 Grid and boundary conditions

In order to achieve a solution where the turbulence and heat flux are fully developed the length of the channel must be of the order $100h$, where h is the channel half-width. In order to correctly resolve the boundary layer turbulence the first cell must be sufficiently small. To calculate this size the friction velocity was taken from the DNS data, the freestream velocity set to $34m/s$ and the static viscosity, μ, set to 10^{-5}. Then the density was calculated

$$\rho = \frac{P}{RT} \tag{5.1}$$

where $P = 10^5 Pa$, $R = 287 J/kgK$ and $T = 300K$. With the density calculated the dynamic viscosity is obtained through $\nu = \mu/\rho$. The smallest cell size, Δ, can then be calculated by

$$y^+_\Delta = \frac{u_\tau \Delta}{\nu} \Longrightarrow \Delta = \frac{y^+_\Delta \nu}{u_\tau} \tag{5.2}$$

The y^+ value closest to the wall, y^+_Δ, is 0.5 for the turbulence model used. The boundary conditions for the channel were set to the following. Inlet: velocity, temperature and pressure specified. Outlet: pressure specified. Both walls were set to isothermal no-slip with a difference in temperature of 30 K (315-285 K).

5.2.2 Calculations

The calculations were executed with a second degree accurate central scheme and low Mach number preconditioning. The results proved to be quite strange however, as seen i figure 5.1. This combination of discretization and boundary condition seemed to overestimate the friction coefficient, equation 5.3, making the balance between centerline and near wall speeds wrong. To investigate the differences in prediction of the friction coefficient between central and upwind schemes a second order accurate upwind scheme was also tested using the same grid and boundary conditions. The upwind scheme is not compatible with low Mach number preconditioning.

$$c_f = 2\left(\frac{u_\tau}{U_m}\right)^2 \tag{5.3}$$

In equation (5.3) U_m is the bulk mean velocity. The results of this investigation were that c_f was equal to 0.0096 and 0.0106 for the upwind and the central scheme, respectively. When using the upwind scheme with the same boundary and initial conditions as in the central case the Reynolds number increased by 22%. More on the reasons for this will follow.

5.2.3 Numerical accuracy in EDGE

During investigation of the dependence of discretization scheme upon c_f prediction it became obvious that EDGE is not very accurate at these low Mach numbers, and the combination of isothermal walls and a central discretization scheme makes EDGE predict c_f in an unphysical way. As seen in figure A.1 the friction coefficient never settles down in this case but decreases rather steadily along the length of the channel and makes a kink at the outlet. The kink at the outlet is probably the boundary condition trying to balance the pressure and velocity here. The pressure distribution close to the wall, as seen in figure A.3, may be the root of evil in this case as it is clear that some kind of instability is present with the combination of central scheme and isothermal walls. The oscillations in P extend to $y^+ \cong 5$ putting the problem mainly in the viscous sublayer, $y^+ < 5$. In this region the Reynolds stresses are negligible compared to viscous stresses making the prediction of viscous stress a promising candidate for investigation. Pressure is related to the density by equation (5.1) but no oscillations are visible either in figure A.5 or in figure 5.1. Since the pressure is almost constant with respect to y, the amplitude of the pressure oscillations is small.

Prediction of turbulent kinetic energy differs between the cases as seen in figure A.4. For the central-isothermal case the level of k in overall is smaller because of a lower Reynolds number but other than that no significant difference is obvious.

c_f predictions were found to be unexpectedly inaccurate for the upwind scheme. A deviation of more than 10% from DNS values is simply not good enough. For this reason a revised wallflux routine for the upwind scheme with a modified boundary condition was tested. The entropy fix, which is a parameter in the upwind scheme that controls the amount of artificial viscosity in low-speed regions, was decreased with a factor of ten from its standard value. As can be seen in figure A.6 the new routine is actually worse than the old one and the tweaked settings does not affect the prediction of c_f at all for this case. The modification of the boundary condition implies how the artificial flux at the wall is controlled, and it is clear from this study that this is an important

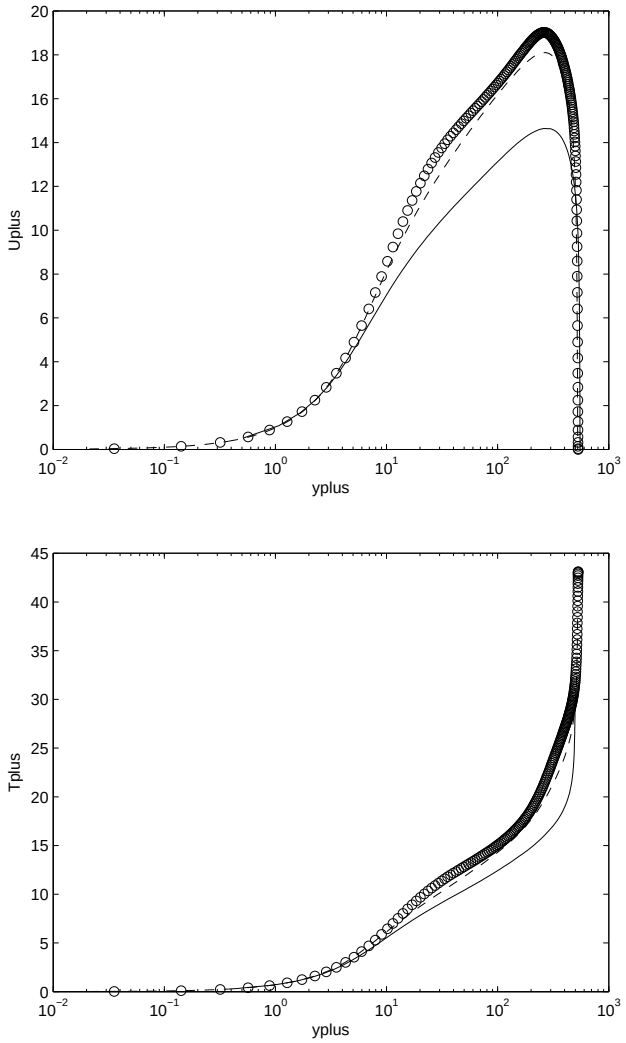

Figure 5.1: EDGE results with EDM and Wallin & Johansson EARSM + Hellsten $k-\omega$ using central scheme, preconditioning and isothermal walls. Top: $\circ$, U^+ from DNS; — , U^+ from EDGE; - - -, U^+ from 1D-solver using EDM. Bottom: $\circ$, Θ^+ from DNS; — , Θ^+ from EDGE; - - -, Θ^+ from 1D-solver using EDM

aspect that needs to be further investigated.

Investigation of the grid resolutions impact on these problems was made by generating a grid with 201 grid points in the direction normal to the walls as opposed to the original grid, that has 101. The grid was generated in such a way that the fist walldistance, y^+, was set to half that of the 101 point case and then the same stretch function was used. The results of the calculations with the finer grid was that c_f decreased by only 3% at $x = 0.06$ compared to the coarse grid when using a central discretization scheme with the isothermal wall boundary condition. When grid resolution goes toward infinity the central and upwind schemes should yield the same results as they, when infinity is reached, are the same. As the 101 point grid is not exactly a coarse grid and the 201 is even less so the results are not very satisfying, one should be able to

see more differences between the two cases and a clearer likeness between the upwind and central scheme. In figure A.3 the oscillations for the fine grid case seem more compressed and confined to a smaller distance, in y^+, from the wall compared to the coarser grid. As a general comment it can be said that the central scheme uses low Mach number preconditioning in this case, an option the the upwind scheme does not have. As the Mach number is quite low this can be expected to be a significant advantage for the central scheme.

5.3 Plane impinging jet

To evaluate the prediction of heatflux by EDGE and the EASFM a DNS study of a plane impinging jet by Hattori et al. [11] was used for comparison. The Reynolds number based on inlet mean velocity and the hydraulic diameter (equal to the width) of the inlet channel was 9120 for the DNS.

$$Re_m = \frac{2V_m D}{\nu} \tag{5.4}$$

5.3.1 Grid and boundary conditions

To make an educated guess of the size of the smallest cell the inlet channel was computed using the 1D-solver tuned to the Reynolds number of the DNS and u_τ was evaluated. Then the Reynolds number based on the mean velocity and the Reynolds number based on the friction velocity was used to predict the friction velocity in the inlet channel of the impinging jet.

$$\frac{Re_{1D}}{Re_{\tau 1D}} = \frac{\frac{U_{1D}L}{\nu}}{\frac{u_{\tau 1D}L}{\nu}} = \frac{U_{1D}}{u_{\tau 1D}} \tag{5.5}$$

This universal relation was used to calculate the friction velocity. Subscript 1D denotes values from the 1D-solver and im denotes impinging jet inlet channel values.

$$\frac{U_{1D}}{u_{\tau 1D}} = \frac{V_{im}}{u_{\tau im}} \Longrightarrow u_{\tau im} = V_{im}\frac{u_{\tau 1D}}{U_{1D}} \tag{5.6}$$

The mean velocity in the inlet channel was set to $30m/s$ and the hydraulic diameter to 1. This together with the definition of the Reynolds number (5.4) gives the dynamic viscosity. The appropriate y^+ for a well resolved computation was chosen to 0.5 and this together with the definition of y^+ gives the size of the first cell with the help of equation (5.2). The grid used for the impinging jet calculations has a smallest cellsize of 0.0017 and a total of 58650 grid points. The boundary conditions were set to the following. Inlet: velocity and temperature specified. Outlet: pressure specified. All the walls except the lower one were set to adiabatic no-slip. As EDGE does not have a constant heatflux boundary condition as that used in the DNS an isotermal no-slip condition was used on the lower wall.

5.3.2 Calculations

The shear layer on the border of the jet creates vortices who are transported downstream by the mean flow. It was found that the central scheme captured this unsteady phenomena and, thus failed to converge to a steady state solution. A second order upwind scheme was tested and proved to stabilize this phenomena and a steady state solution could be obtained. The dampening effect that the upwind scheme gives could also have been obtained by making the grid coarser in the shear layer and running a central scheme. This approach would aim at not resolving the creation of the vortices but was not

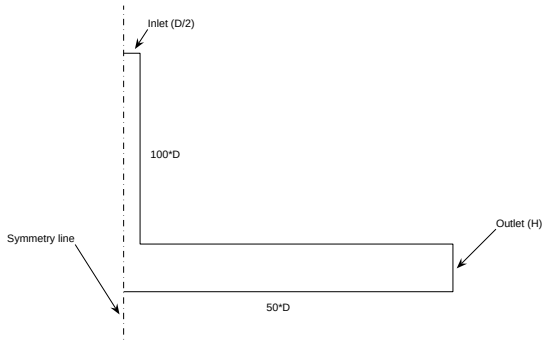

Figure 5.2: Computational domain for the impinging jet (not to scale). D=1, H=2D. Inlet channel has 60*140 gridpoints, outlet 201*250 gridpoints

tested because of the good results from the upwind scheme. Time accurate calculations, though maybe the most intuitively promising approach, leads to additional problems. First and foremost is that this approach aims at resolving the instantaneous turbulent field something that, as turbulence per definition is three-dimensional and the computational field is two-dimensional, is quite doubtful. Moreover, a RANS approach is in principal not valid for time accurate calculations when the resolved time scale is of the same order as the turbulence. As the instantaneous field is not of interest in this case anyway timeaccurate calculations were abandoned.

5.3.3 Comparison of some turbulence models

During the setup of the impinging jet calculations the Wilcox k-ω turbulence model was used as it is less sensitive than the EARSM type models. In figure 5.3 two of the differences between EARSM and k-ω models are illustrated. The k-ω model predicts higher turbulent kinetic energy at the point where the jet strikes the wall which might expect to affect heat transfer in this area. The reason for this is that the production of turbulent kinetic energy in a standard eddy-viscosity model such as the $k-\omega$ model is proportional to the square of the strain rate tensor, S_{ij}^* in equation (3.7), whereas in the EARSM it is directly proportional. The shear layer at the edge of the jet also varies between the two models with EARSM predicting slightly more turbulent kinetic energy in this area. This can be because of the higher turbulent kinetic energy at the impinging point and thus it may not be an independent phenomenon.

Other differences are that the recirculating zone is larger in the EARSM calculation, making the reattachment of the flow occur further away from the jet as seen in figure 5.4. Another effect is that the velocity magnitude close to the lower wall stays high further down for the EARSM due to the squeezing effect by the larger recirculation. The effect all this has on the heat transfer can be displayed by plotting the Nusselt number,

$$Nu = \frac{2q_w D}{\lambda \Delta \Theta} \tag{5.7}$$

where q_w is the wall heat flux, D the width of the inlet channel, λ the thermal conductivity and $\Delta\Theta$ the temperature difference between the inlet and the

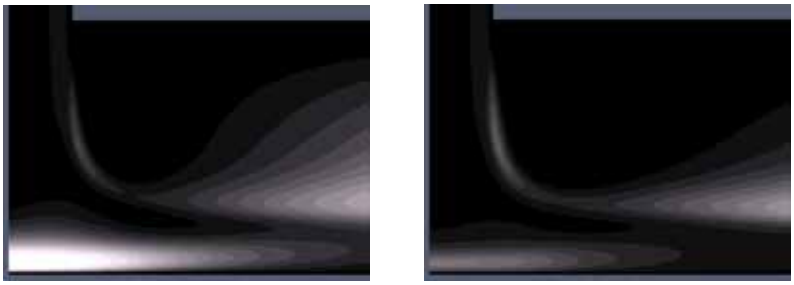

Figure 5.3: Comparison of Wilcox k-ω (left) and Wallin & Johansson EARSM + Hellsten k-ω(right), prediction of turbulent kinetic energy

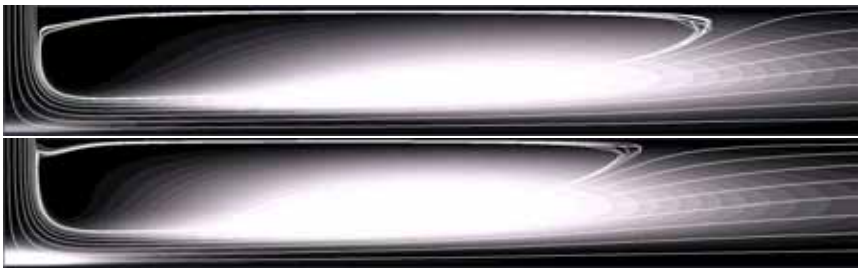

Figure 5.4: Comparison of Wallin & Johansson EARSM + Hellsten k-ω(top) and Wilcox k-ω, visualization of differences in recirculating flow size and reattachment point location. Greyscale is turbulent kinetic energy

impinging wall. As can be seen in figure 5.5, the Nusselt number for the k-ω model is higher where it predicted a higher turbulent kinetic energy than the EARSM. Also the Nusselt number is lower compared to the EARSM from $x/D \approx 5$ due to that the lower velocity close to the wall in this area generates less turbulence.

5.4 Issues on the implementation of EASFM in EDGE

After the channel case had been set up in EDGE the idea was to implement the EASFM model into EDGE. This, however, proved to be rather more complicated than expected. Implementation was first attempted using code-generating software related to the 1D-solver mentioned earlier. This software is capable of translating algebraic equations into fortran code compatible with the EDGE routines. Testing revealed convergence problems as the solutions blew up within a few iterations leading to suspicions of numerical stability problems. In order to investigate this a numerical stability analysis was made.

5.4.1 Numerical stability analysis

Consider the diffusive term of the governing equation for temperature.

$$\frac{\partial T}{\partial t} = \frac{\partial}{\partial x_j}\left(\alpha_{ij}\frac{\partial T}{\partial x_j}\right) \tag{5.8}$$

Now let T instead denote a small perturbation around a valid solution, the equations for the perturbation and the solution are the same as the equation for the solution is linear. To investigate the behavior of the perturbation, or

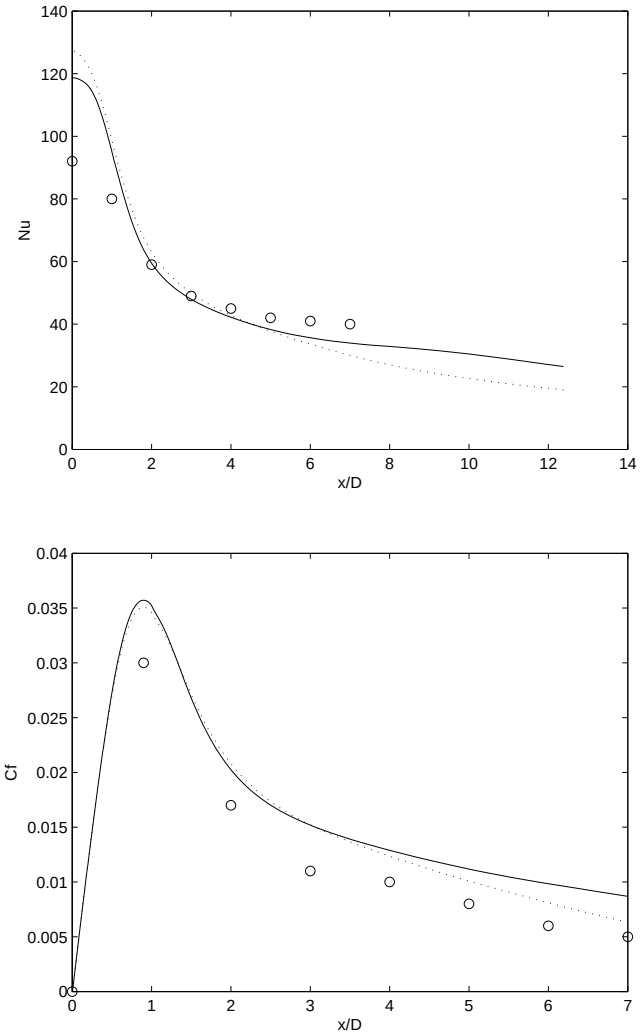

Figure 5.5: Comparison of $k-\omega$, Wallin & Johansson EARSM + Hellsten k-ω and DNS. Top: Nusselt number from impinging jet case. Bottom: Friction coefficient from impinging jet case. —, Wallin & Johansson EARSM + Hellsten k-ω; ..., Wilcox k-ω; o, DNS

error, in time the energy norm of equation (5.8) is considered. First equation (5.8) is multiplied with T and integrated over the computational domain.

$$\int_V T\frac{\partial T}{\partial t}dV = \int_V T\frac{\partial}{\partial x_i}\left(\alpha_{ij}\frac{\partial T}{\partial x_j}\right)dV \tag{5.9}$$

which can be rewritten as

$$\int_V \frac{\partial}{\partial t}\left(\frac{1}{2}T^2\right)dV = \int_V \left[-\frac{\partial T}{\partial x_i}\alpha_{ij}\frac{\partial T}{\partial x_j} + \frac{\partial}{\partial x_j}\left(\alpha_{ij}\frac{\partial}{\partial x_j}\left(\frac{1}{2}T^2\right)\right)\right]dV \tag{5.10}$$

and

$$\frac{\partial}{\partial t}\int_V \frac{1}{2}T^2 dV = -\int_V \frac{\partial T}{\partial x_i}\alpha_{ij}\frac{\partial T}{\partial x_j}dV + \int_{\delta V}\alpha_{ij}\frac{\partial}{\partial x_j}\left(\frac{1}{2}T^2\right)n_i d\delta \tag{5.11}$$

The energy norm of the perturbation says that the error will decrease in time if the right hand side of equation (5.11) is negative. The last term must be considered when setting boundary conditions but the focus here will be on the volume term. The first term is strictly negative if

$$\frac{\partial T}{\partial x_i}\alpha_{ij}\frac{\partial T}{\partial x_j} \tag{5.12}$$

is strictly positive and this is the case if α_{ij} is positive definite. Now, according to equation (2.3) α_{ij} is

$$\alpha_{ij} = (1 - c_{\theta 4})A_{ik}^{-1}\overline{u_k u_j}\frac{k}{\varepsilon} \tag{5.13}$$

and since A_{ij} is positive definite A_{ij}^{-1} is this as well. The Reynolds stress tensor, $\overline{u_i u_j}$, is also positive definite. However, an inner product of two positive definite tensors is not necessarily positive definite and, thus, α_{ij} is not strictly positive definite and a numerical instability may occur.

As a way to attempt to solve the stability problem an effective eddy-diffusivity may be obtained by minimizing the error $e = e_i e_i$, where

$$e_i = \alpha_{ij}\frac{\partial T}{\partial x_j} - \alpha^{eff}\frac{\partial T}{\partial x_i} \tag{5.14}$$

by the least squares method by setting $\partial e/\partial \alpha^{eff} = 0$.

$$e = e_i e_i = (\alpha^{eff})^2\frac{\partial T}{\partial x_i}\frac{\partial T}{\partial x_i} - 2\alpha^{eff}\frac{\partial T}{\partial x_i}\alpha_{ij}\frac{\partial T}{\partial x_j} + \alpha_{ij}\frac{\partial T}{\partial x_j}\alpha_{ik}\frac{\partial T}{\partial x_k} \tag{5.15}$$

$$\frac{\partial e}{\partial \alpha} = 0 = 2\alpha^{eff}\frac{\partial T}{\partial x_i}\frac{\partial T}{\partial x_i} - 2\frac{\partial T}{\partial x_i}\alpha_{ij}\frac{\partial T}{\partial x_j} \tag{5.16}$$

which gives

$$\alpha^{eff} = \frac{\frac{\partial T}{\partial x_i}\alpha_{ij}\frac{\partial T}{\partial x_j}}{\frac{\partial T}{\partial x_k}\frac{\partial T}{\partial x_k}} \tag{5.17}$$

Now, α_{ij} can be written as

$$\alpha_{ij} = \alpha^{eff}\delta_{ij} + (\alpha_{ij} - \alpha^{eff}\delta_{ij}) \tag{5.18}$$

and with equation (5.18) the relation (5.12) can be written as

$$\frac{\partial T}{\partial x_i}\alpha_{ij}\frac{\partial T}{\partial x_j} = \frac{\partial T}{\partial x_l}\alpha^{eff}\frac{\partial T}{\partial x_l} + \frac{\partial T}{\partial x_i}(\alpha_{ij} - \alpha^{eff}\delta_{ij})\frac{\partial T}{\partial x_j} \tag{5.19}$$

Now, the first term on the right hand side together with equation (5.17) reads

$$\frac{\partial T}{\partial x_l}\alpha^{eff}\frac{\partial T}{\partial x_l} = \frac{\frac{\partial T}{\partial x_l}\frac{\partial T}{\partial x_i}\alpha_{ij}\frac{\partial T}{\partial x_j}\frac{\partial T}{\partial x_l}}{\frac{\partial T}{\partial x_k}\frac{\partial T}{\partial x_k}} = \frac{\partial T}{\partial x_i}\alpha_{ij}\frac{\partial T}{\partial x_j} \tag{5.20}$$

this means that the last term in equation (5.19) must be equal to zero. This implies that, as it disappears in the stability criteria, the second term in equation (5.18) will not contribute to the stability. Now a modified diffusion tensor can be proposed as

$$\alpha_{ij}^{*} = \max(\alpha^{eff}, 0)\delta_{ij} + (\alpha_{ij} - \alpha^{eff}\delta_{ij}) \tag{5.21}$$

which will preserve stability also in the case that α_{ij} is not positive definite.

6 Comparison of EDGE and Fluent

In parallell with the work on this thesis the author attended the course "applied computational fluid dynamics", 5C1213, at KTH. The chosen project was to use Fluent [10] to predict turbulence and heat transfer in an impinging jet. The Fluent results in this report are based on lessons learned during this project. A new mesh was used for the thesis and more time was invested in details regarding the treatment of the boundary layer in Fluent.

6.1 Grid and boundary conditions

The idea behind this comparison at first was to compare Fluent and EDGE with the same input, or as close as possible. However, due to that it proved impossible to obtain a solution in Fluent with a similar grid to the EDGE case a more simple grid was used together with Fluent. The problem was that Fluent refused to produce a turbulent boundary layer in the inlet channel and thus the inlet became a laminar channel flow making the two cases too different. The only explanation to the problems seems to be that the grid was too fine and somehow this made the solver predict a laminar solution in the inlet channel. A more coarse grid with a $\Delta y_1^+ = 1$ was constructed and solved the problem. Gridgeneration was handled with Gambit, a mesh/preprocessing software that is bundled with Fluent. Boundary conditions were, with the exception of inlet pressure, set to the same values as in the EDGE case. Inlet pressure was adjusted to give the correct Reynolds number at the inlet channel.

6.2 Calculations

Fluent calculations were made with three turbulence models, the realizable $k-\varepsilon$, standard $k-\varepsilon$ and the $k-\omega$ model. The results are visible in figure 6.1 where the data is presented together with results from the EDGE $k-\omega$ calculations as well as DNS data. The data seems to agree rather well with the DNS, only the spike at $x/D \approx 0.5$ slightly disturbs the agreement. The spike is located at the interface between two boundaries and might be related to how the boundary conditions are treated in Fluent. It may also be the result of inadequate grid resolution and if so it may be fixed by further grid refinement. As can be seen in figure 6.2 the prediction of turbulent kinetic energy is rather different between the models. The shear layer on the jet is in the case of the $k-\varepsilon$ models predicted to be rather wide giving the jet in itself a more "flared" appearance than the $k-\omega$. This may be connected to the difference in recirculation zone shape as the $k-\varepsilon$ models give smaller, more concentrated and less stretched in the x-direction, zones as opposed to the $k-\omega$. The differences between the two $k-\varepsilon$ models are that the realizable seems to predict a smaller amount of k at the impinging point and in general is half way between the standard $k-\varepsilon$ and the $k-\omega$ model. For the $k-\omega$ model Fluent and EDGE results in figure 5.3 compare well.

The Fluent calculations were, as mentioned, computed with a rather coarse grid compared to the EDGE case. Moreover the built-in grid refinement tools in Fluent were not utilized. All this suggests that the computational capabilities of Fluent may not have been fully utilized in this study and that the results could be improved in a more detailed study.

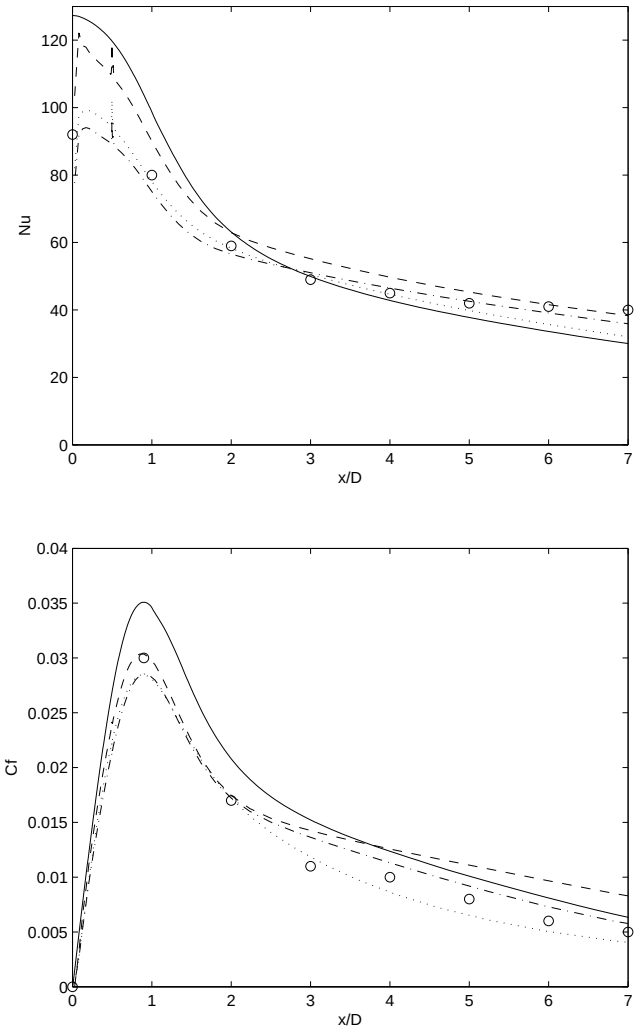

Figure 6.1: Comparison of EDGE and Fluent. Top: Nusselt number, bottom: Friction coefficient. —, EDGE $k-\omega$; -.-., Fluent realizable $k-\varepsilon$; ..., Fluent standard $k-\varepsilon$; - - -, Fluent $k-\omega$: o, DNS

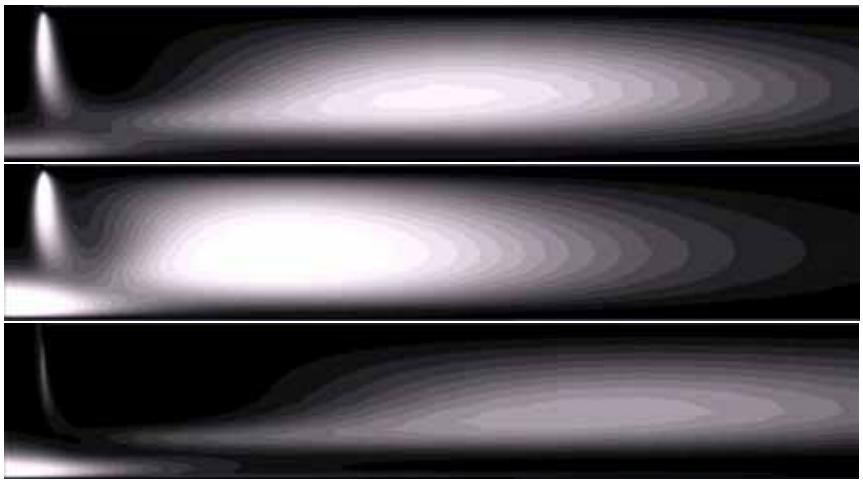

Figure 6.2: Visualization of prediction of turbulent kinetic energy in Fluent calculations. Top: realizable $k-\varepsilon$. Middle: standard $k-\varepsilon$. Bottom: $k-\omega$

7 Conclusions

The EASFM proposed by Högström Wallin and Johansson [15] [12] was originally proposed together with the Wallin and Johansson EARSM [4] with near-wall corrections for capturing also the near-wall behavior of the Reynolds stress tensor and scalar (or heat) flux vector. Is this report a simplistic approach containing no special near wall treatment is taken to scalar flux and turbulence modelling, only a minor recalibration of the EASFM was needed. It was found that, for turbulent channel flow, this approach produces reasonably accurate results if one is not specifically considered in the details of the near-wall turbulence statistics. The mean scalar profile is reasonaby well predicted with both the EDM and the EASFM models where the latter produces the best results.

The comparisons made between turbulence models confirmed previous knowledge regarding the differences in characteristics of the prediction of turbulent kinetic energy. Also, the comparison showed surprisingly small differences in prediction of c_f and Nusselt number between the $k-\omega$ and EARSM turbulence models in the impinging jet case calculated with EDGE.

The calculations made using EDGE show clearly the problem of producing accurate numerical results depending on the numerical scheme and boundary condition used. Results using a isothermal wall boundary condition together with a central discretization scheme seems to produce numerical instabilities in EDGE resulting in unphysical prediction of the pressure close to the walls. Also, prediction of c_f in the channel flow case show an overprediction of c_f by more than 10%. Despite using a rather coarse, non-refined, grid Fluent results better agreed with the DNS reference data compared with EDGE results.

The original goal of this thesis, to implement a EASFM model into EDGE, encountered problems related to numerical stability. A stability analysis identified likely reasons for the instabilities and a modified diffusion tensor is proposed. Further work with, and testing of, this modified diffusion tensor could provide a working implementation of the EASFM scalar flux model in EDGE.

A more detailed investigation of the numerical accuracy issues resulting in the overprediction of c_f when using isothermal boundary conditions and a central discretization scheme is needed in order to better understand the reasons behind this. Also, the unphysical prediction of the oscillation in the pressure requires further investigation. Finally, the Fluent calculations may not fully utilize the capabilities of the solver. Grid refinement and more time is needed in order to produce calculations that can be said to represent this solvers capabilities.

Dr Hattori, Nagoya Institute of Technology, is gratefully acknowledged for kindly providing us with data from the simulation [11].

A Plots regarding numerical accuracy in EDGE

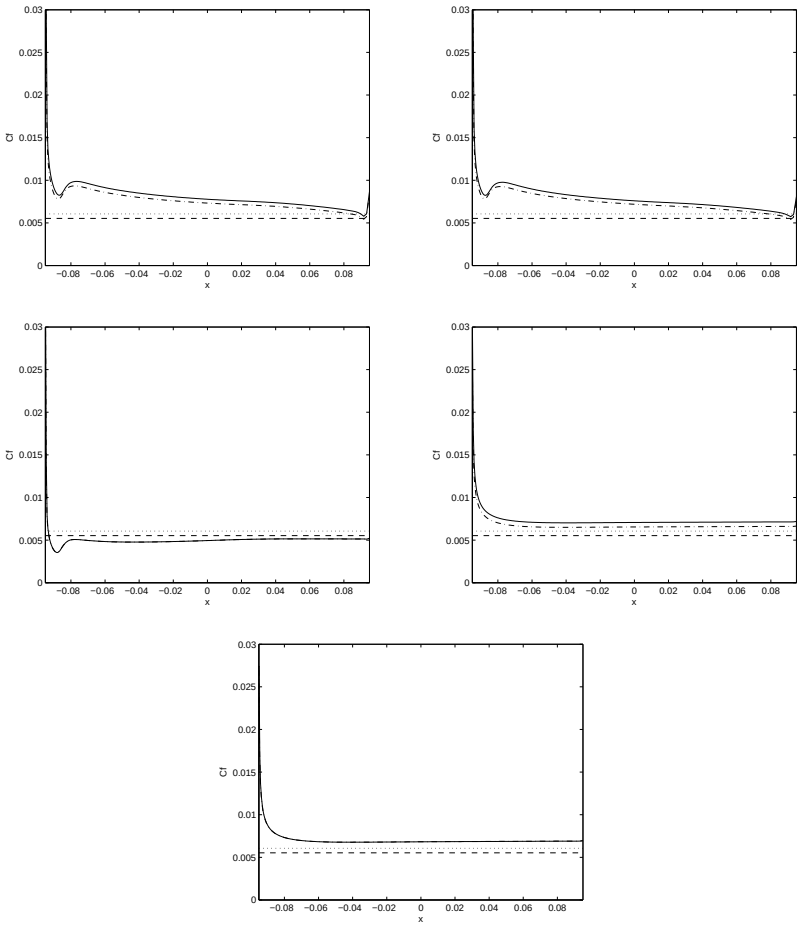

Figure A.1: Friction coefficient, c_f. Top row left: central scheme with isothermal walls, Re = 5064. Top row right: central scheme with isothermal walls, fine grid, Re = 5106. Middle row left: central scheme with adiabatic walls, Re = 6424. Middle row right: upwind scheme with isothermal walls, Re = 6402. Bottom row: upwind scheme with adiabatic walls, Re = 6422. —, Lower wall; .-, Upper wall; ..., 1D-solver; - -, DNS

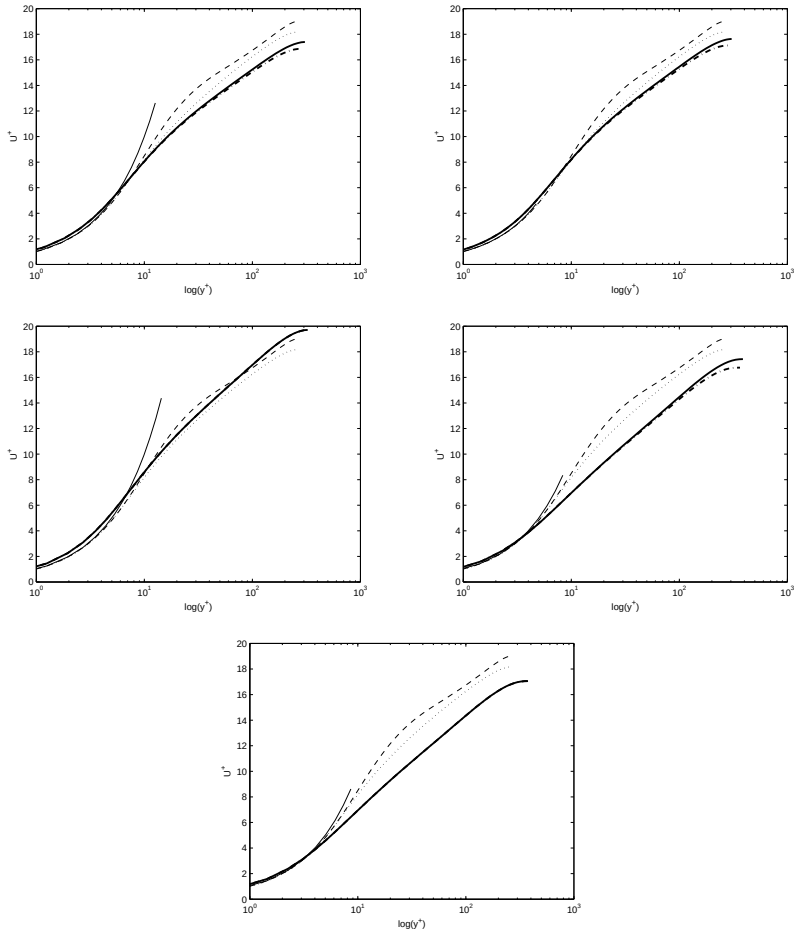

Figure A.2: U^+ versus $log(y^+)$. Top row left: central scheme with isothermal walls, Re = 5064. Top row right: central scheme with isothermal walls, fine grid, Re = 5106. Middle row left: central scheme with adiabatic walls, Re = 6424. Middle row right: upwind scheme with isothermal walls, Re = 6402. Bottom row: upwind scheme with adiabatic walls, Re = 6422. — (thick line), Lower wall; .- (thick line), Upper wall; ..., 1D-solver; - -, DNS; —, $U^+ = y^+$

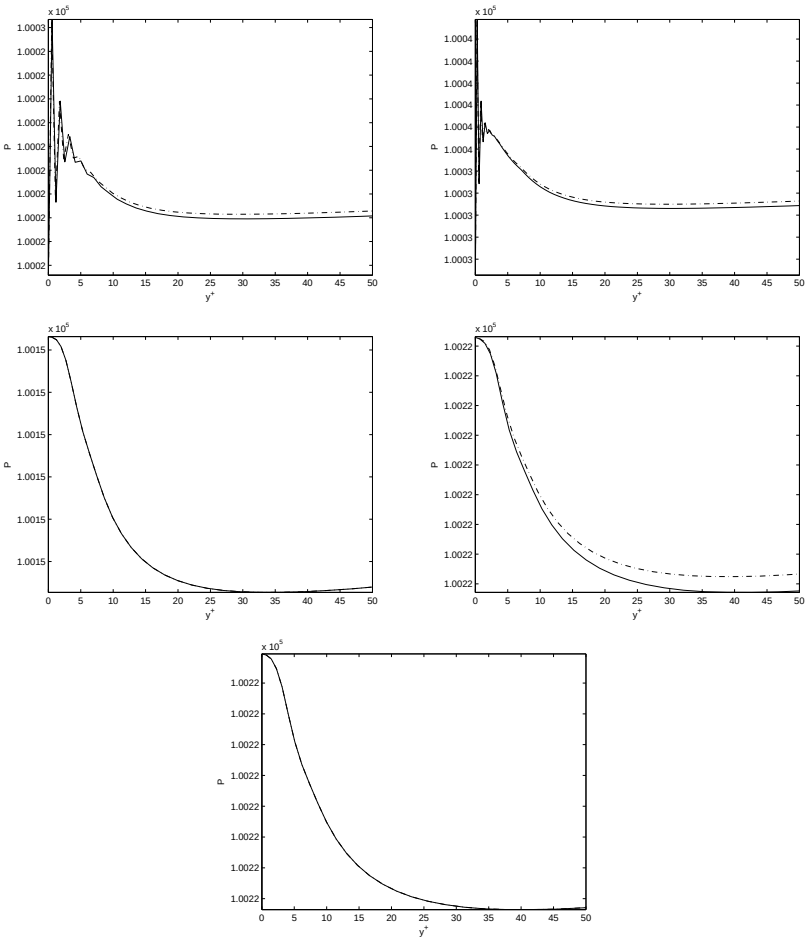

Figure A.3: Pressure. Top row left: central scheme with isothermal walls, Re = 5064. Top row right: central scheme with isothermal walls, fine grid, Re = 5106. Middle row left: central scheme with adiabatic walls, Re = 6424. Middle row right: upwind scheme with isothermal walls, Re = 6402. Bottom row: upwind scheme with adiabatic walls, Re = 6422. —, Lower wall; .-, Upper wall; ..., 1D-solver; - -, DNS

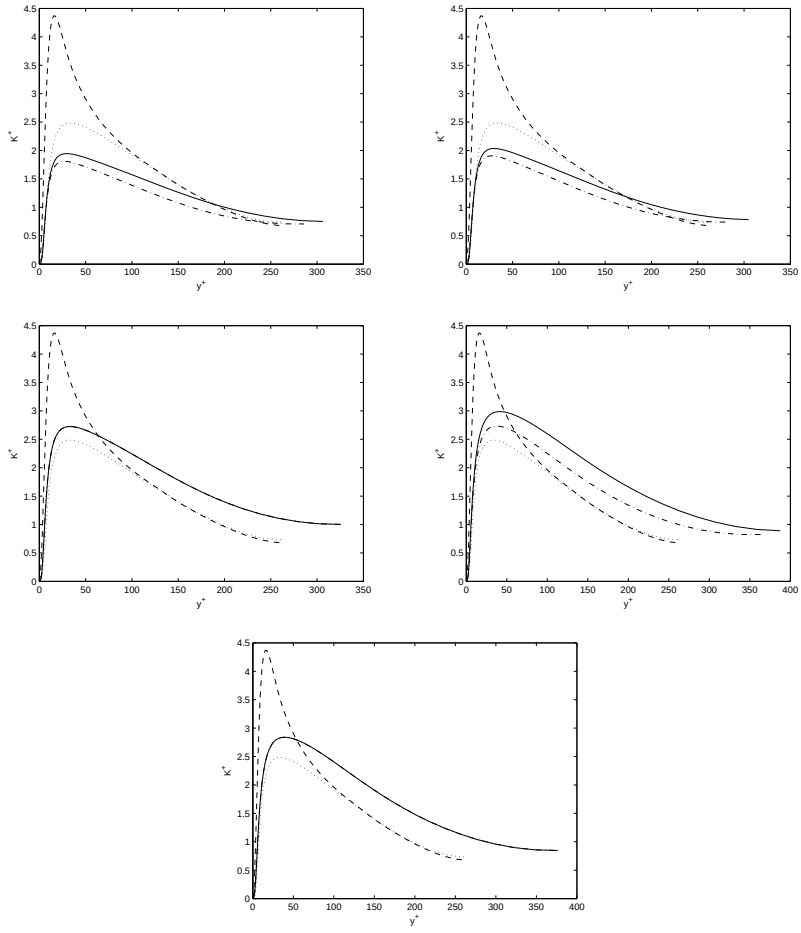

Figure A.4: K^+ versus $log(y^+)$. Top row left: central scheme with isothermal walls, Re = 5064. Top row right: central scheme with isothermal walls, fine grid, Re = 5106. Middle row left: central scheme with adiabatic walls, Re = 6424. Middle row right: upwind scheme with isothermal walls, Re = 6402. Bottom row: upwind scheme with adiabatic walls, Re = 6422. —, Lower wall; .-, Upper wall; ..., 1D-solver; - -, DNS

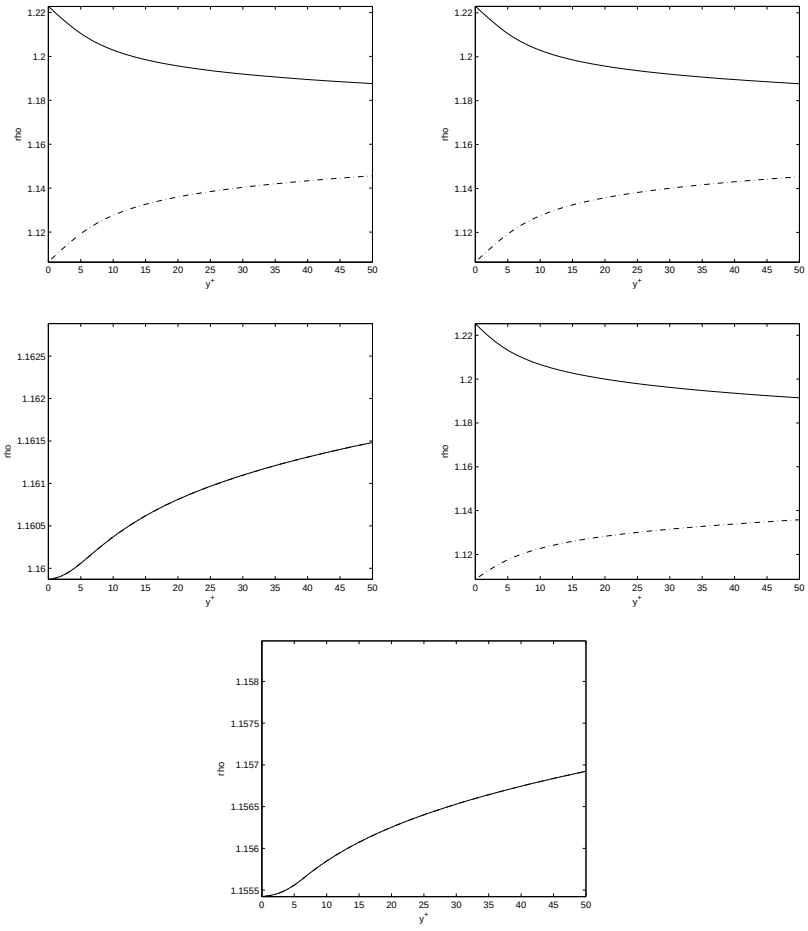

Figure A.5: Density, ρ . Top row left: central scheme with isothermal walls, Re = 5064. Top row right: central scheme with isothermal walls, fine grid, Re = 5106. Middle row left: central scheme with adiabatic walls, Re = 6424. Middle row right: upwind scheme with isothermal walls, Re = 6402. Bottom row: upwind scheme with adiabatic walls, Re = 6422. —, Lower wall; .-, Upper wall; ..., 1D-solver; - -, DNS

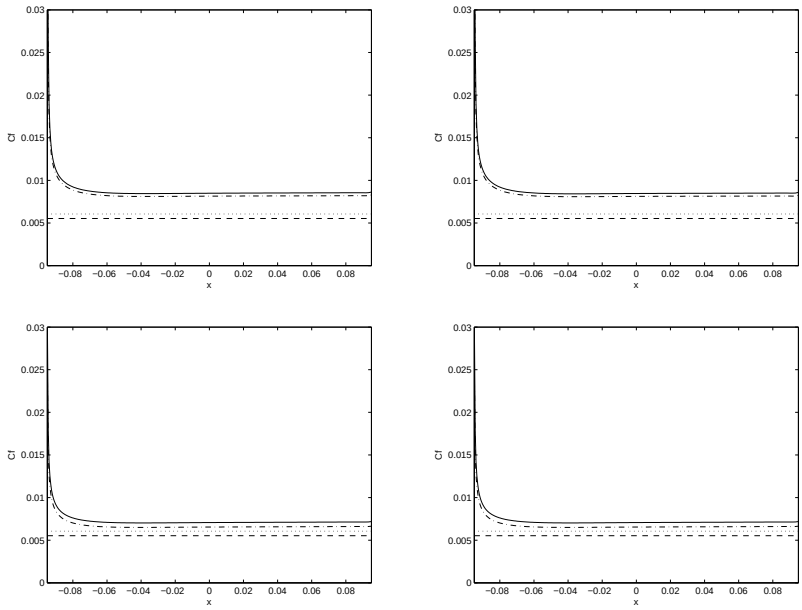

Figure A.6: Friction coefficient, c_f. Comparison of different wallflux computational routines and entropy fix settings, upwind scheme with isothermal walls . Top left: New routine, standard entropy fix. Top right: New routine, tweaked entropy fix. Bottom left: Old routine, standard entropy fix. Bottom right: Old routine, tweaked entropy fix. —, Lower wall; .-, Upper wall; ..., 1D-solver; - -, DNS

Bibliography

[1] Richardson, L.F. Weather Prediction by Numerical Process. *Cambridge*, 1922.

[2] Kolmogorov, A.N. The local structure of turbulence in incompressible viscous fluid for very large Reynolds number. *Dokl. Acad. Nauk SSSR*, (1941).

[3] Wikström, P.M., Wallin, S. & Johansson, A.V. Derivation and investigation of a new explicit algebraic model for the passive scalar flux. *Physics of fluids*, **1**2, 3 (Mar. 2000), 688–702.

[4] Wallin, S. & Johansson, A.V. An explicit algebraic Reynolds stress model for incompressible and compressible flows. *J. Fluid Mech.*, **4**03 (2000), 89–132.

[5] Durbin, P. Application of a near-wall turbulence model to boundary layers and heat transfer. *Int J. Heat Fluid Flow*, **1**4 (1993), 316–323.

[6] Maplesoft Homepage http://www.maplesoft.com.

[7] Tysell L.G. & Hedman S.G. Towards a general Three-dimensional Grid Generation System. *ICAS-88-4.7.4* (1988), 1048-1058.

[8] Eliasson, P. EDGE, a Navier-Stokes Solver for Unstructured Grids. Scientific Report FOI-R–0298–SE. Computational Aerodynamics Department, Aeronautics Division, FOI..

[9] EDGE Homepage http://www.edge.foi.se.

[10] Fluent Homepage http://www.fluent.com.

[11] Hattori, H. & Nagano, Y. Direct numerical simulation of turbulent heat transfer in plane impinging jet. *Int J. Heat Fluid Flow*, **2**5 (2004), 749–758.

[12] Högström, C.M. Explicit algebraic scalar flux modelling for CFD. *FFA TN 2000-66* (2000)

[13] Menter, F.R. Two-equation eddy-viscosity turbulence models for engineering applications. *AIAA Journal*, **3**2 (8), 1598-1605 (1994)

[14] Hellsten, A. New Advanced k-ω Turbulence Model for High-Lift Aerodynamics. *AIAA Journal*, **4**3 (9), 1857-1869 (September 2005)

[15] Högström, C.M., Wallin, S. & Johansson A.V. Passive Scalar Flux Modelling for CFD. *2 nd Int. Symp. on Turbulence and Shear Flow Phenomena (TSFP2), Stockholm* (2001)